Journal of Luminescence ∎ (∎∎∎∎) ∎∎∎–∎∎∎

Contents lists available at ScienceDirect

Journal of Luminescence

journal homepage: www.elsevier.com/locate/jlumin

Energy level structure and optical dephasing under magnetic field in Er^{3+}:$LiYF_4$ at 1.5 μm

Robert Marino [a], Ivan Lorgeré [b,1], Olivier Guillot-Noël [a,1], Hervé Vezin [c], Alessandra Toncelli [d], Mauro Tonelli [d], Jean-Louis Le Gouët [b], Philippe Goldner [a,*]

[a] PSL Research University, Chimie ParisTech – CNRS, Institut de Recherche de Chimie Paris, 75005 Paris, France
[b] Laboratoire Aimé Cotton, CNRS UMR 9188 Université Paris-Sud, Bât. 505, 91405 Orsay cedex, France
[c] LASIR CNRS UMR 8516, Université de Lille, France
[d] NEST, Nanoscience Institute – CNR, Dipartimento di Fisica, Università di Pisa, Largo B. Pontecorvo, 3 56127 Pisa, Italy

ARTICLE INFO

Article history:
Received 30 October 2014
Received in revised form
3 March 2015
Accepted 8 March 2015

ABSTRACT

Er^{3+}:$LiYF_4$ is a material where optical inhomogeneous linewidths are smaller than hyperfine splittings, which could be advantageous for quantum information processing protocols. We investigated the Zeeman and hyperfine structures under magnetic field by optical spectroscopy at 1.5 μm and found a good agreement with calculations based on crystal field wavefunctions. Since Zeeman splittings have a non-linear dependance on the magnetic field, this calculations could be useful to estimate energy level structures for arbitrary field strengths and orientations. Coherence lifetimes have been measured on a 100 ppm erbium doped sample under a 2.2 T magnetic field. Values up to 4.7 μs have been observed, with an exponential decay of the echo intensity as a function the pulse delay.

1. Introduction

Rare earth doped crystals have recently raised a strong interest for quantum information processing applications, either in the field of quantum computing [1] or optical quantum memories [2–4]. This is due to the long optical coherence lifetimes that can be reached in these materials because of the shielding of *f* electrons by closed shells [5,6]. For example, this allows one to use high bandwidth, photon echo based protocols, for quantum memories. Moreover, it is also possible to take advantage of ground state nuclear spin transitions with even longer coherence lifetimes and to which optical coherences can be transferred. Using specific magnetic fields [7,8] and dynamic decoupling techniques [3,9,10], it is possible to observe coherence lifetimes in the 100 ms–30 s range. However, isolating optical transitions between hyperfine levels is difficult and usually requires complex optical pumping sequences [11,12]. This is because the hyperfine splittings are smaller than the optical inhomogeneous linewidth in many crystals. This is however not the case in a few rare earth doped halide crystals like Ho^{3+}:$LiYF_4$ [13], Ho^{3+}:CaF_2 [14], Er^{3+}:$CsCdBr_3$ [15], Nd^{3+}:$LiYF_4$ [16] and Er^{3+}:$LiYF_4$ [17], where optical linewidths can be as narrow as a few 10 MHz. In this case, optical transitions between hyperfine levels are directly observed in transmission, which in turn could considerably simplify the implementation of quantum computing and memory protocols.

The 1.5 μm transition of Er^{3+} ions is compatible with the transmission window of silica optical fibers and erbium doped materials have been extensively studied in the field of optical telecommunication, mainly as optical amplifiers. Quantum information processing using photons at 1.5 μm would also be very advantageous, if only to be able to use sophisticated optical telecom technologies. Moreover, quantum cryptography can already be operated through standard optical telecom fibers [18].

Er^{3+} is a Kramers ion with a $4f^{11}$ configuration. The 1.5 μm transition is found between the ground $^4I_{15/2}$ and first excited $^4I_{13/2}$ multiplets. The maximum ground state *g* factor is typically in the 8–15 range, depending on material and magnetic field orientation. Er has only one non-zero nuclear spin isotope, ^{167}Er (22.9% abundance), for which $I = 7/2$ and $g_n = -0.1618$. Several studies have investigated quantum memories protocols in Er^{3+}:Y_2SiO_5 at 1.5 μm [19,20]. In Ref. [21], electromagnetic induced transparency was demonstrated at the same wavelength in Er^{3+}:Y_2SiO_5 using ground and excited state ^{167}Er hyperfine levels. However, identification of the necessary three level Λ system was difficult because of ^{167}Er large nuclear spin (7/2) and a hyperfine splitting comparable to the optical inhomogeneous linewidth. Because of this, holeburning spectra were extremely complex and could be only partially analyzed with the help of a detailed electron paramagnetic resonance (EPR) study [22]. In Er^{3+}:$LiYF_4$ single crystal, the 1.5 μm optical

* Corresponding author.
E-mail address: philippe.goldner@chimie-paristech.fr (P. Goldner).
[1] In memoriam.

http://dx.doi.org/10.1016/j.jlumin.2015.03.003
0022-2313/

inhomogeneous linewidth is smaller than the typical hyperfine splitting at zero field [23]. Detailed studies of the spectral and coherent properties of the red $^4I_{15/2} - {}^4F_{9/2}$ transition have been reported, showing that coherence lifetimes close to 10 μs could be observed at high magnetic fields [17,24–27]. Optical absorption and coherence lifetime of the $^4I_{15/2} - {}^4I_{13/2}$ transition at 1.5 μm have also been briefly reported in a review paper [28].

In this paper, we present the Zeeman energy level structures and the coherence properties of the $^4I_{15/2} - {}^4I_{13/2}$ 1.5 μm transition under magnetic field.

2. Experimental

Samples of 0.01% Er:$LiYF_4$ with natural isotopic abundance were grown by the Czochralski method. A $1 \times 1 \times 5$ mm^3 parallelepiped, with one 1×5 mm^2 face perpendicular to the c axis, could be placed under a ≈ 2.2 T magnetic field produced by permanent NdFeB magnets. The field was perpendicular or parallel to c. The crystal and magnetic assembly were inserted into a Janis helium bath cryostat. The sample temperature could be set between 1.6 and 20 K.

Light propagated along the longest dimension of the sample. Transmission spectra were recorded using the broad band amplified spontaneous emission from an erbium doped fiber amplifier (EDFA) and an optical spectrum analyzer (0.01 nm resolution). Higher resolution spectra were obtained using a 100 kHz linewidth (over 10 ms) home made extended cavity diode laser [29] which was boosted by the EDFA to a maximum of 4 mW at the crystal under investigation. Laser pulses for photon echoes experiments were generated by an acousto optic modulator. Transmitted light was detected with an amplified photodiode (Thorlabs PDA255).

CW electron paramagnetic resonance (CW EPR) was performed on a X-band Bruker Elexsys 500 spectrometer at 5 K.

3. Energy level structure under magnetic fields

In $LiYF_4$, erbium ions substitute yttrium ions in one crystallographic site of S_4 point symmetry. Since Er^{3+} has an odd number of electrons, all crystal field levels are doubly degenerate unless a magnetic field is applied. In each $^{2S+1}L_J$ multiplet, crystal field levels are numbered in order of increasing energy, starting from 0. In the following, we focus on transitions from Zeeman levels of the ground $^4I_{15/2}(0)$ doublet to those of the excited $^4I_{13/2}(0)$ and $^4I_{13/2}(1)$ doublets when a static magnetic field B_0 is applied. The corresponding labels are given in Fig. 1.

3.1. Optical spectroscopy and crystal field analysis

Polarized absorption spectra for B_0 magnetic field along or perpendicular to the c axis are shown in Figs. 2 and 3. In the latter case, the spectrum showed no clear dependence on light polarization, and only the π ($E \| c$, $B \perp c$) spectrum is presented. Transitions are labelled according to Fig. 1 scheme. At high magnetic fields, deviations can be expected from the linear Zeeman effect [27] and we analyzed the energy splittings by crystal field calculations.

Following Ref. [30], we used a free ion Hamiltonian including the magnetic M^k and T^k parameters. For the crystal field Hamiltonian, the actual Er^{3+} point symmetry, S_4, was approximated by D_{2d}, as the imaginary part of the B_6^4 crystal field parameter is small. Using the free ion parameters of Ref. [30], we optimized the crystal field parameters with respect to the 26 experimental crystal field level energies of the ^4I term [30] (final rms deviation 5.5 cm^{-1}) and calculated $g_\|$ and $g_\perp$ factors of the ground $^4I_{15/2}(0)$ and excited $^4I_{13/2}(0)$

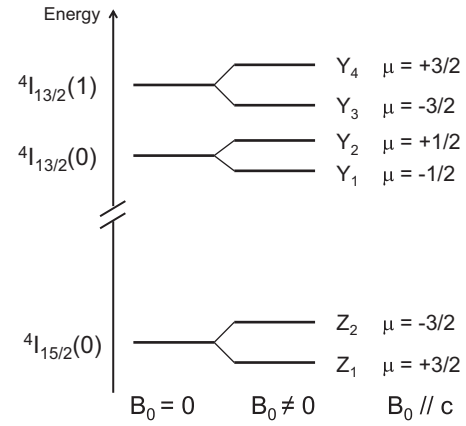

Fig. 1. Partial diagram of Er^{3+} crystal field and Zeeman energy levels showing relevant labels and crystal field quantum numbers in the case of $B_0 \| c$.

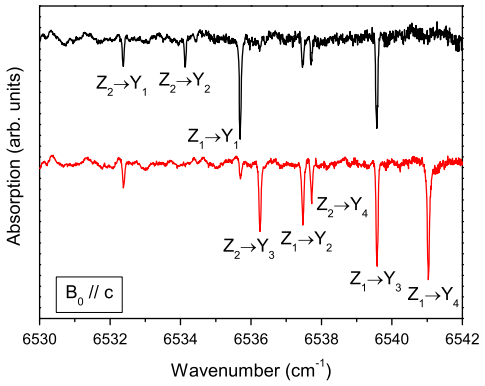

Fig. 2. Absorption spectrum with $B_0 \| c$. Upper trace: π polarization ($E \| c$, $B \perp c$); lower trace: σ polarization ($E \perp c$, $B \| c$). $T = 5$ K.

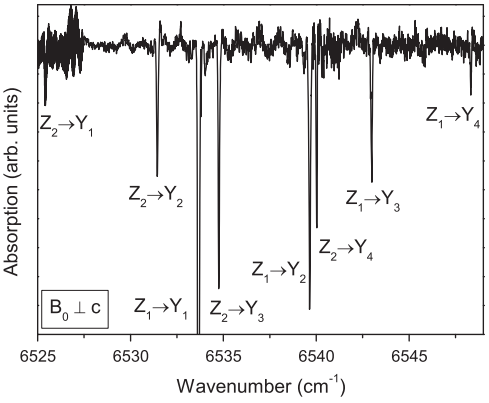

Fig. 3. π polarized absorption spectrum with $B_0 \perp c$. $T = 20$ K.

Table 1
Crystal field (CF) parameters and g factors of $^4I_{15/2}(0)$ and $^4I_{13/2}(0)$ doublets.

CF param.	Value (cm^{-1})	Level	g factor	Exp.	Calc.
B_0^2	405	$^4I_{15/2}(0)$	$g_\|$	3.147	3.433
B_0^4	−769		$g_\perp$	8.105	8.150
B_4^4	−886	$^4I_{13/2}(0)$	$g_\|$	1.37[a]	1.62
B_0^6	−36		$g_\perp$		7.45
B_4^6	−654				

[a] From Ref. [32].

states. A good agreement was found with g factors determined by CW EPR (Table 1) as well as with other experiments and calculations [31,32].

Fig. 4 shows the variation of the Zeeman level energies of the $^4I_{15/2}(0)$, $^4I_{13/2}(0)$ and $^4I_{13/2}(1)$ doublets for magnetic fields up to 2.5 T and parallel to c or to a (or b) axes. Nonlinear dependences are mainly observed for the excited states with fields larger than ≈ 0.5 T perpendicular to c. This nonlinear behavior is due to mixing of the crystal field levels by the magnetic field. When allowed by symmetry, mixing is stronger between close lying levels and becomes significant when their energy separation is of the order of the Zeeman one. These conditions are fulfilled for the excited states with B_0 perpendicular to c (i): the $^4I_{13/2}(0)$ and $^4I_{13/2}(1)$ levels are separated by only $\approx 5\ cm^{-1}$ at zero field and $g_\perp = 7.45$, corresponding to a Zeeman splitting of 8.7 cm^{-1} at 2.5 T; (ii) as the field is not along c, the total Hamiltonian has a lower symmetry than S_4 (or D_{2d}), relaxing the selection rules on level mixing. When the field is parallel to c, the lowest energy level which can be mixed with $^4I_{13/2}(0)$ (resp. $^4I_{13/2}(1)$) is $^4I_{13/2}(3)$ (resp. $^4I_{13/2}(2)$) with an energy separation of 136 cm^{-1} (resp. 31 cm^{-1}). The nonlinear behavior is therefore weaker in this case. This is also observed for $B_0 \| c$ or $B_0 \perp c$ in the ground state, where $^4I_{15/2}(0)$ and $^4I_{15/2}(1)$ are separated by 22 cm^{-1}.

For B_0 parallel to the c-axis, the experimental Zeeman splittings $Z_1 - Z_2$, $Y_1 - Y_2$, $Y_3 - Y_4$ are respectively 3.31, 1.75 and 1.46 cm^{-1}. The best theoretical fit was obtained with a 2.11 T field oriented along c, close to the estimated magnitude of the experimental field ($B_0 \approx$ 2.2 T) . The calculated splittings were 3.31, 1.59 and 2.08 cm^{-1}, in reasonable agreement with experimental values. When B_0 was perpendicular to c, the experimental Zeeman splittings were 8.26, 6.05 and 5.28 cm^{-1} and the best theoretical ones 8.26, 6.17 and 4.82 cm^{-1}. The latter were obtained with a 2.2 T magnetic field oriented 18° away from a (or b) in the (a,b) plane. Indeed, the magnetic field was strong enough to lower the axial symmetry in the calculations.

We also investigated the polarization of the transitions between Zeeman levels in the $B_0 \| c$ case where the original axial site symmetry is preserved. Each calculated level was characterized by its crystal field quantum number μ, which can take the values $\pm 1/2$ and $\pm 3/2$ in D_{2d} symmetry (Fig. 1). The selection rules for electric and magnetic dipole transitions are given in Table 2. As the $^4I_{13/2} \leftrightarrow {}^4I_{15/2}$ transition obeys the $\Delta J = 1$ selection rule, magnetic dipole processes are allowed.

The polarized spectra shown in Fig. 2 are in good agreement with theory. For example, the $Z_2 \rightarrow Y_2$ line is only observed in the π spectrum ($\mu = -3/2 \rightarrow \mu = 1/2$ electric dipole transition) whereas the $Z_2 \rightarrow Y_3$ and $Z_1 \rightarrow Y_4$ lines are σ polarized ($\mu = -3/2 \rightarrow \mu = -3/2$ and $\mu = +3/2 \rightarrow \mu = +3/2$ magnetic dipole transitions). The $Z_1 \rightarrow Y_1$ line is mainly π polarized ($\mu = +3/2 \rightarrow \mu = -1/2$ electric dipole transition) but a small σ component is also observed. This may be due to a small misorientation of the magnetic field.

3.2. Hyperfine structure

Hyperfine structure of $^{167}Er^{3+}$ was investigated by recording transmission spectra with a narrow linewidth (100 kHz over the experiments time scale) tunable laser. The zero magnetic field spectrum centered at 1530.37 nm (vacuum) of the $^4I_{15/2}(0) \rightarrow {}^4I_{13/2}(0)$ transition is shown in Fig. 5(a) and is similar to the one reported in Ref. [23], although the spectral resolution was limited to 150 MHz in this previous work. A part from the intense line corresponding to the $I=0$ nuclear spin isotopes, several weaker lines are observed. The transition denoted by a star is due to Er^{3+} ions with one nearest neighbour ^6Li isotope [33]. Other lines correspond to transitions between hyperfine

Table 2
Selection rules for electric (E) and magnetic (B) dipole transitions in D_{2d} symmetry.

μ	$-1/2$	$1/2$	$-3/2$	$3/2$
$-1/2$	$B \| c$	$B,\ E \perp c$	$B,\ E \perp c$	$E \| c$
$1/2$	$B,\ E \perp c$	$B \| c$	$E \| c$	$B,\ E \perp c$
$-3/2$	$B,\ E \perp c$	$E \| c$	$B \| c$	$B,\ E \perp c$
$3/2$	$E \| c$	$B,\ E \perp c$	$B,\ E \perp c$	$B \| c$

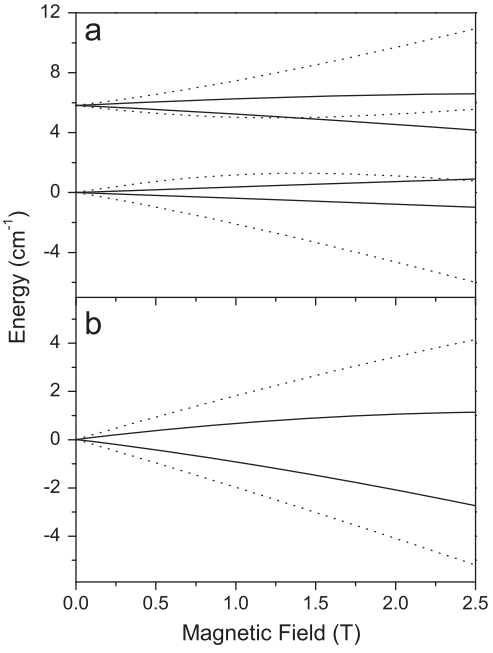

Fig. 4. Calculated Zeeman level energies as a function of B_0 magnetic field parallel to c (solid lines) or to a (dashed lines). (a) $^4I_{15/2}(0)$, (b) $^4I_{13/2}(0)$ and $^4I_{13/2}(1)$.

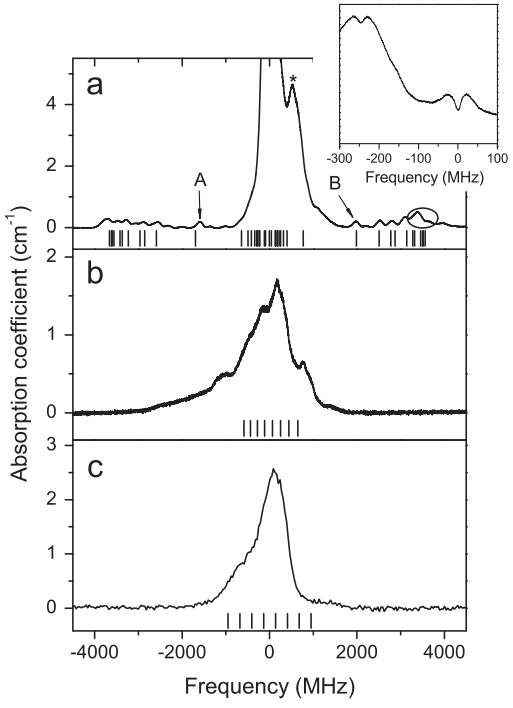

Fig. 5. High resolution absorption spectra at 10 K. (a) $^4I_{15}(0) \rightarrow {}^4I_{13/2}(0)$ transition at zero magnetic field. Inset: example of a central hole burnt in a transition between hyperfine levels and the corresponding side hole. A, B, and ⋆ labels see text. (b) (Resp. (c)) $Z_1 \rightarrow Y_1$ transition absorption spectrum for $B_0 \| c$ (resp. $B_0 \perp c$).

Please cite this article as: R. Marino, et al., J. Lumin. (2015), http://dx.doi.org/10.1016/j.jlumin.2015.03.003

levels of $^{167}Er^{3+}$ ions. At zero magnetic field, the hyperfine interaction partly lifts the electronic and nuclear spin degeneracy leading to 9 hyperfine levels, two singlets and seven doublets, for each crystal field level. The linewidth of well separated hyperfine lines is ≈ 170 MHz. Since Er^{3+} concentration is only 100 ppm, this inhomogeneous broadening is mainly due to the random distribution of Li and Er isotopes [17]. Indeed a linewidth of 16 MHz was observed in a 50 ppm doped $^{170}Er^{3+}$: $^{7}LiYF_4$ [28].

As some lines overlap and may be difficult to precisely identify, we used holeburning spectroscopy to clarify the hyperfine structure. Holes were burned in transitions well separated from the intense zero nuclear spin transition. The side holes which were observed correspond to transitions starting from the same ground state hyperfine level as the central hole, but connecting to different excited state hyperfine levels. An example of a side hole at −250 MHz from the central hole is shown in the inset of Fig. 5(a). The depth of the side holes was comparable to the central ones, indicating that branching ratios between transitions are significant. This is due to the non-diagonal matrix elements of the hyperfine interaction which mix levels with $\Delta M_I = \pm 1$ where M_I is the nuclear spin projection. The holes lifetimes in the A and B hyperfine transitions (see Fig. 5(a)) were 270 and 70 μs respectively. This is explained by population relaxation within the ground state hyperfine levels, as the holes burnt in the zero nuclear spin line had a lifetime of 10 ms, corresponding to the $^4I_{13/2}(0)$ excited state lifetime. The short lifetime of holes burnt in transitions between hyperfine levels prevented the observation of anti-holes since no population redistribution within ground state hyperfine levels could last longer than the excited state lifetime.

Burning holes in all the hyperfine lines resulted in the excited state hyperfine structure which is shown in Fig. 6. We then used the crystal field level parameters determined above to obtain the hyperfine level energies. Calculations were performed adding nuclear and hyperfine interactions to the previous free ion, crystal field and electronic Zeeman Hamiltonian. Quadrupolar interactions were neglected [31]. In the hyperfine interaction constant expression, the mean value of the f electron orbital radii $\langle r^3 \rangle$ was adjusted to fit experimental data. With $\langle r^3 \rangle = 10.17\, a_0^3$ where a_0 is the Bohr atomic radius, calculated hyperfine energies for the excited state were in good agreement with experimental ones (Fig. 6). Transition energies between ground and excited state hyperfine levels were also calculated, taking into account the $\Delta M_I = 0$ on the nuclear spin projection. This leads to 45 transitions which are in good agreement with most of the major features of the experimental spectrum (Fig. 5).

High resolution spectra of the $Z_1 \rightarrow Y_1$ transition were then recorded under magnetic fields (Fig. 5(b) and (c)). Broad lines (≈ 2 GHz), showing some spectral features, are observed. This broadening is probably due a combination of magnetic field inhomogeneities and overlap between close lying hyperfine transitions. Indeed, for $B_0 \| c$, the mean energy separation of transitions between hyperfine levels is only 180 MHz, close to the zero field inhomogeneous linewidth (≈ 170 MHz) (Fig. 5(b)). For $B_0 \perp c$, the mean separation reaches 300 MHz, suggesting that the lines could be resolved in a highly homogeneous magnetic field (Fig. 5(c)). Since the hyperfine interaction is much smaller than the electronic Zeeman one at high magnetic fields, only $\Delta M_I = 0$ transitions are considered. Holes with lifetimes of 10 ms were burnt into the $Z_1 \rightarrow Y_1$ transition but no side holes or anti-holes were observed, in agreement with the above selection rule.

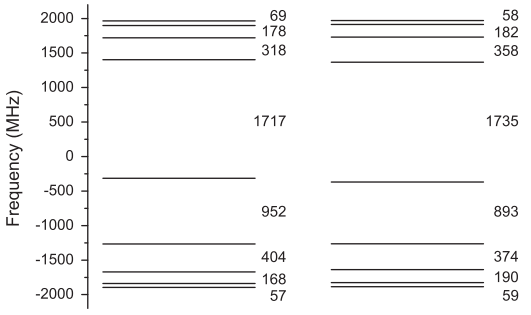

Fig. 6. Experimental (left) and calculated (right) hyperfine structures of the $^4I_{13/2}(0)$ level at zero magnetic field. Splittings (in MHz) between successive levels are shown on the right of the schemes.

4. Optical dephasing

Optical dephasing was measured using two pulse photon echoes. At zero magnetic field no echo was observed on any transition. At 2.2 T, we were able to measure coherence lifetimes for the Z_1–Y_1 transition of 1.4 and 4.7 μs for $B_0 \| c$ and $B_0 \perp c$ respectively (Fig. 7). The echo intensity decays exponentially over the studied time range which is limited, especially in the $B_0 \| c$ case, by the weakness of the echo signal.

Previous studies on the $^4I_{15/2}(0)$–$^4F_{9/2}(0)$ transition concluded that the main dephasing mechanism was the perturbation of the coherently prepared Er^{3+} ions by magnetic field fluctuations [24,26]. When the external field B_0 is low, those fluctuations result from the flips of both the Er^{3+} ground state electronic spins and the F^- nuclear spins. As the magnetic field B_0 is raised, the echo decay slows down, becomes non-exponential and finally independent of B_0. While Er^{3+} electronic spins get strongly polarized by the static field, F^- nuclear spins flip dynamics are not directly affected because of their small gyromagnetic ratio (40 MHz/T), as compared to Er^{3+} one (14 GHz/T for $g = 3.15$). However, because of Er^{3+} large magnetic moment, F^- ions close to an Er^{3+} ion have their nuclear transition shifted away from F^- ions at larger distance. As a consequence F^- spins undergo the fewer flip-flop transitions as they are closer to an Er^{3+} ion. Hence Er^{3+} ions are affected by magnetic fluctuations with different rates and magnitudes. Fast flip-flops of F^- ions at large distance cause small perturbations, while slower flips of closer F^- ions produce larger fluctuations. This is the so-called frozen core effect which results in a non-exponential echo decay [25,24].

In the $B_0 \perp c$ configuration, we observe an exponential decay of the echo intensity at 2.2 T in a 100 ppm Er:$LiYF_4$ sample (Fig. 7). A non-exponential decay has been reported in a 50 ppm doped sample under a 5.4 T magnetic field at 1.3 K with a phase memory time $T_M = 12$ μs and a stretch factor $x = 2.3$ [28]. Since at this large fields dephasing is dominated by F^- nuclear spin flips (see above), coherence loss in our experiments is likely to be partly due to Er^{3+} electron spin flips. However, non-exponential decays were also recorded on the $^4I_{15/2}(0)$–$^4F_{9/2}(0)$ transition with 200 ppm Er^{3+}

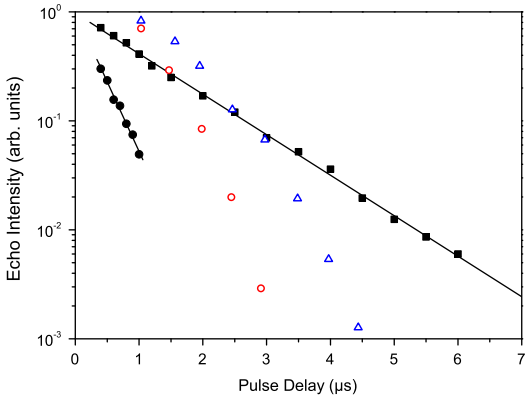

Fig. 7. Two pulse echo intensity decays as a function of the delay between pulses . $^4I_{15/2}(0)$–$^4I_{13/2}(0)$ transition: $B_0 \approx 2.2$ T; squares: $B_0 \perp c$, filled circles: $B_0 \| c$; T = 1.6 K. $^4I_{15/2}(0)$–$^4F_{9/2}(0)$ transition (from Ref. [26]): $B_0 \perp c$; open circles: $B_0 = 2.0$ T, open triangles: $B_0 = 2.3$ T; $T = 1.5$ K.

concentration [26], in similar magnetic field conditions (Fig. 7). This suggests that other mechanisms, like instantaneous spectral diffusion, may also have to be taken into account to explain our results.

We note that our echo signal decays more slowly than in Ref. [26] at delays larger than $\approx$2–2.5 μs. This is consistent with the expected smaller sensitivity of the $^4I_{15/2}(0)$–$^4I_{13/2}(0)$ to magnetic fluctuations. That sensitivity is proportional to the difference $|g-g'|$ between the g factors of the lowest Zeeman levels (Z_1 and Y_1) [24] of the ground and excited states. On $^4I_{15/2}(0)$–$^4F_{9/2}(0)$, $|g-g'|\approx 8$ whereas $|g-g'|=2$ on $^4I_{15/2}(0)$–$^4I_{13/2}(0)$. However, we unexpectedly observe faster decay at delays <2.5 μs.

In the $B_0\|c$ configuration, the data reported in Ref. [26] were not obtained in the same magnetic field range as ours. The echo decay is still exponential, and faster than in the $B_0\perp c$ configuration. The smaller Zeeman splitting of the ground state doublet for $B_0\|c$ ($\approx 3\ cm^{-1}$ instead of $\approx 8\ cm^{-1}$ for $B_0\perp c$, according to Fig. 4) indicates that Er^{3+} spins are less polarized and suggests that Er^{3+} spin flipping might dominate the relaxation process in these conditions.

5. Conclusion

We have determined part of the low temperature structure of Zeeman energy levels under strong magnetic fields (2.2 T) for the $^4I_{15/2}-{}^4I_{13/2}$ transition at 1.5 μm in Er^{3+}:$LiYF_4$. A crystal field analysis was able to reproduce this structure with deviations lower than 1 cm^{-1}, which suggests that it can be used for other magnetic fields strength or orientations. The zero field hyperfine structure of the $^4I_{13/2}(0)$ excited state has been determined by holeburning spectroscopy and could also be very well reproduced by calculations. Under magnetic field, we were unable to resolve the hyperfine structure, probably because of inhomogeneities in the magnetic field. However, calculations predict that this should be possible given the hyperfine splittings and linewidths (170 MHz at zero field), especially for $B_0\perp c$. The use of isotopically pure samples, both in ^{167}Er and ^7Li, could also be very useful in reducing the inhomogeneous linewidth.

Coherence lifetimes up to 4.7 μs have been measured. The echo intensity exponentially decays as a function of the pulse delay. This is not consistent with the previously observed [26] non-exponential behavior on the $^4I_{15/2}-{}^4F_{9/2}$ transition. Hence, the dephasing mechanism has still to be clarified.

Concerning possible applications to quantum information processing, two important properties have still to be determined. First, we could not observe any ground state population transfer by hole burning under magnetic field. This may be due to selection rules which in turn can be relaxed by a specific magnetic field [34,35]. Second, ground state hyperfine coherence lifetimes have to be measured since it is these transitions which will be used for long time storage of quantum information.

Acknowledgments

The research leading to these results has received funding from the European Union's Seventh Framework Programme FP7/2007-2013/ under REA Grant agreements no. 287252 (CIPRIS, People Programme-Marie Curie Actions).

References

[1] L. Rippe, B. Julsgaard, A. Walther, Y. Ying, S. Kröll, Phys. Rev. A 77 (2008) 022307.
[2] W. Tittel, M. Afzelius, T. Chanelière, R. Cone, S. Kröll, S. Moiseev, M. Sellars, Laser Photon. Rev. 4 (2010) 244.
[3] M. Lovrić, D. Suter, A. Ferrier, Ph. Goldner, Phys. Rev. Lett. 111 (2013) 020503.
[4] F. Bussières, C. Clausen, A. Tiranov, B. Korzh, V.B. Verma, S.W. Nam, F. Marsili, A. Ferrier, P. Goldner, H. Herrmann, C. Silberhorn, W. Sohler, M. Afzelius, N. Gisin, Nat. Photonics 8 (2014) 775.
[5] R.M. Macfarlane, J. Lumin. 100 (2002) 1.
[6] A. Perrot, Ph. Goldner, D. Giaume, M. Lovrić, C. Andriamiadamanana, R.R. Gonçalves, A. Ferrier, Phys. Rev. Lett. 111 (2013) 203601.
[7] E. Fraval, M.-J. Sellars, J.J. Longdell, Phys. Rev. Lett. 92 (2004) 077601.
[8] M. Lovric, P. Glasenapp, D. Suter, B. Tumino, A. Ferrier, P. Goldner, M. Sabooni, L. Rippe, S. Kröll, Phys. Rev. B 84 (2011) 104417.
[9] E. Fraval, M.-J. Sellars, J.J. Longdell, Phys. Rev. Lett. 95 (2005) 030506.
[10] A. Arcangeli, M. Lovrić, B. Tumino, A. Ferrier, Ph. Goldner, Phys. Rev. B 89 (2014) 184305.
[11] M. Nilsson, L. Rippe, S. Kröll, R. Klieber, D. Suter, Phys. Rev. B 70 (2004) 214116.
[12] O. Guillot-Noël, P. Goldner, F. Beaudoux, Y. Le Du, J. Lejay, A. Amari, A. Walther, L. Rippe, S. Kröll, Phys. Rev. B 79 (2009) 155119.
[13] N.I. Agladze, M.N. Popova, G.N. Zhizhin, V.J. Egorov, M.A. Petrova, Phys. Rev. Lett. 66 (1991) 477.
[14] J.-P.R. Wells, G.D. Jones, M.F. Reid, M.N. Popova, E.P. Chukalina, Mol. Phys. 102 (2004) 1367.
[15] E. Chukalina, M. Popova, E. Antic-Fidancev, J. Chaminade, Phys. Lett. A 258 (1999) 375.
[16] R.M. Macfarlane, R.S. Meltzer, B.Z. Malkin, Phys. Rev. B 58 (1998) 5692.
[17] R.M. Macfarlane, A. Cassanho, R.S. Meltzer, Phys. Rev. Lett. 69 (1992) 542.
[18] D. Stucki, N. Gisin, O. Guinnard, G. Ribordy, H. Zbinden, New J. Phys. 4 (2002) 41.
[19] B. Lauritzen, J. Minář, H. de Riedmatten, M. Afzelius, N. Sangouard, C. Simon, N. Gisin, Phys. Rev. Lett. 104 (2010) 080502.
[20] J. Dajczgewand, J.-L. Le Gouët, A. Louchet-Chauvet, T. Chanelière, Opt. Lett. 39 (2014) 2711.
[21] E. Baldit, K. Bencheikh, P. Monnier, S. Biraudeau, J.A. Levenson, O. Guillot-Noël, P. Goldner, Opt. Lett. 39 (2014) 2711.
[22] O. Guillot-Noël, P. Goldner, Y.L. Du, E. Baldit, P. Monnier, K. Bencheikh, Phys. Rev. B 74 (2006) 214409.
[23] M.N. Popova, E.P. Chukalina, B.Z. Malkin, S.K. Saikin, Phys. Rev. B 61 (2000) 7421.
[24] R. Macfarlane, R. Wannemacher, D. Boye, Y. Wang, R. Meltzer, J. Lumin. 48–49 (1991) 313.
[25] J. Ganem, Y.P. Wang, D. Boye, R.S. Meltzer, W.M. Yen, R.M. Macfarlane, Phys. Rev. Lett. 66 (1991) 695.
[26] R.S. Meltzer, J. Ganem, Y.P. Wang, D. Boye, W.M. Yen, D.P. Landau, R. Wannemacher, R.M. Macfarlane, J. Lumin. 53 (1992) 1.
[27] R. Wannemacher, D. Boye, Y.P. Wang, R. Pradhan, W. Grill, J.E. Rives, R.S. Meltzer, Phys. Rev. B 40 (1989) 4237.
[28] C.W. Thiel, T. Böttger, R.L. Cone, J. Lumin. 131 (2011) 353.
[29] V. Crozatier, G. Gorju, F. Bretenaker, J.-L. Le Gouët, I. Lorgeré, C. Gagnol, E. Ducloux, Appl. Phys. Lett. 89 (2006) 261115.
[30] M. Couto dos Santos, E. Antic-Fidancev, J. Gesland, J. Krupa, M. Lemaître-Blaise, P. Porcher, J. Alloys Compd. 275–277 (1998) 435.
[31] J.P. Sattler, J. Nemarich, Phys. Rev. B 4 (1971) 1.
[32] S.M. Kulpa, J. Phys. Chem. Solids 36 (1975) 1317.
[33] E. Chukalina, M. Popova, S. Korableva, R. Abdulsabirov, Phys. Lett. A 269 (2000) 348.
[34] M. Afzelius, M.U. Staudt, H. de Riedmatten, N. Gisin, O. Guillot-Noël, P. Goldner, R. Marino, P. Porcher, E. Cavalli, M. Bettinelli, J. Lumin. 130 (2010) 1566.
[35] O. Guillot-Noël, P. Goldner, E. Antic-Fidancev, J.-L. Le Gouët, Phys. Rev. B 71 (2005) 174409.

Please cite this article as: R. Marino, et al., J. Lumin. (2015), http://dx.doi.org/10.1016/j.jlumin.2015.03.003